01 Feb 2011

Observation of Strong Resonant Behavior in the Inverse Photoelectron Spectroscopy of Ce Oxide

James G. Tobin

Sw Yu

Brandon W. Chung

George Daniel Waddill
Missouri University of Science and Technology, waddill@mst.edu

et. al. For a complete list of authors, see https://scholarsmine.mst.edu/phys_facwork/1185

Recommended Citation

J. G. Tobin et al., "Observation of Strong Resonant Behavior in the Inverse Photoelectron Spectroscopy of Ce Oxide," *Physical review B: Condensed matter and materials physics*, vol. 83, no. 8, pp. 085104-1-085104-9, American Physical Society (APS), Feb 2011.
The definitive version is available at https://doi.org/10.1103/PhysRevB.83.085104

Observation of strong resonant behavior in the inverse photoelectron spectroscopy of Ce oxide

J. G. Tobin,[1,*] S. W. Yu,[1] B. W. Chung,[1] G. D. Waddill,[2] L. Duda,[3] and J. Nordgren[3]
[1]*Lawrence Livermore National Laboratory, Livermore, California 94550, USA*
[2]*Missouri University of Science and Technology, Rolla, Missouri 65401, USA*
[3]*Uppsala University, Uppsala, Sweden*

(Received 23 February 2010; revised manuscript received 10 November 2010; published 11 February 2011)

X-ray emission spectroscopy and resonant inverse photoelectron spectroscopy (RIPES) have been used to investigate the photon emission associated with the Ce $3d_{5/2}$ and Ce $3d_{3/2}$ thresholds. Strong resonant behavior has been observed in the RIPES of a Ce oxide near the 5/2 and 3/2 edges.

DOI: 10.1103/PhysRevB.83.085104 PACS number(s): 78.70.En, 71.20.Eh, 71.20.Ps

I. INTRODUCTION

Inverse photoelectron spectroscopy (IPES) and its high-energy variant, bremsstrahlung isochromat spectroscopy (BIS), are powerful techniques that permit a direct interrogation of the low-lying unoccupied electronic structure of a variety of materials. Despite being handicapped by counting rates that are approximately four orders of magnitude less that the corresponding electron spectroscopies [photoelectron spectroscopy (PES) and x-ray photoelectron spectroscopy (XPS)] both IPES (Refs. 1–5) and BIS (Refs. 6–8) have a long history of important contributions. Over time, an additional variant of this technique has appeared, where the kinetic energy (KE) of the incoming electron and photon energy ($h\nu$) of the emitted electron are roughly the same magnitude as the binding energy of a core level of the material in question. Under these circumstances and in analogy to resonant photoelectron spectroscopy, a cross-section resonance can occur, giving rise to resonant inverse photoelectron spectroscopy (RIPES).[9–13] Here, we report the observation of RIPES in an *f*-electron system, specifically at the $3d_{5/2}$ and $3d_{3/2}$ thresholds of a Ce oxide. (See Fig. 1.)

The resonant behavior of the Ce 4*f* structure at the 3*d* thresholds has been addressed before, including studies of the utilization of the technique as a probe of electron correlation in a variety of Ce compounds.[12] Interestingly, the first RIPES work on rare earths dates back to 1974, albeit under conditions that left the state of the surface and near-surface regions undefined. Although they did not use the more modern terminology of "RIPES," it is clear that RIPES was actually first performed in 1974 by Liefeld, Burr, and Chamberlain on both La- and Ce-based materials.[9] In these experiments, the La and Ce metallic samples were attached to the anode of an x-ray tube and the x-ray emission (XES) characteristics were measured by using a two-crystal monochromator. The pressure in the x-ray tube was quoted as being below 2×10^{-8} Torr. They did indeed observe resonant behavior at the $M\alpha$ ($3d_{5/2}$) and $M\beta$ ($3d_{3/2}$) thresholds. In fact, our results here will confirm the measurements made upon the Ce-based sample used by Liefeld *et al*. However, the state of the Ce sample surface and near-surface regions are quite undefined in the study in Ref. 9. For example, the authors suggest that they are probing Ce metal, because they cannot see any evidence of an O $K\alpha$ (1*s*) XES line. However, they do report the observation of a F $K\alpha$ (1*s*) line, possibly owing to the utilization of cerium fluoride in the sample preparation. Later, they tried to address these issues in a new ultrahigh vacuum system.[13] Based upon our results, it is clear that their original sample surface was oxidized, using the word here in its more general context as in having lost electrons to the oxidizing agent, although whether the structure is an oxide or fluoride remains unclear. In any case, the primacy of Liefeld and co-workers in these measurements should be noted.

Cerium and cerium oxide have been studied with a variety of spectroscopic techniques under UHV conditions. This includes BIS,[6] PES,[6,14–18] x-ray absorption spectroscopy (XAS),[19–21] electron energy loss spectroscopy (EELS),[6,20,22,23] and resonant XES,[24,25] to name just a few. We will compare our results to those of other spectroscopies, as will be discussed below.

The remainder of this paper will be as follows. In Sec. II, the experimental details will be described. In Sec. III, the determination of sample quality with XES and the RIPES results will each be presented and discussed, within the context of the mechanisms of RIPES and XES, as shown in Fig. 2. Finally, Sec. IV will contain a summary and conclusions.

II. EXPERIMENTAL

The experiments were carried out on site at Lawrence Livermore National Laboratory, using a spectrometer[26] with capabilities for performing spin-resolved Fano spectroscopy,[27] IPES, or BIS,[28] sample cleaning with argon-ion bombardment, and sample heating and cooling in an UHV environment.

The polycrystalline Ce sample was oxidized by exposure to air at ambient pressures. After introduction to the UHV system, the oxidized sample was bombarded with Ar ions to clean the topmost surface regions. The specific details are as follows. The polycrystalline Ce foil (99.9% of purity, 0.1 mm of thickness, from Alfa Aesar) was cut into a piece with the size of 7×10 mm^2. One side of the Ce foil was polished with a very fine sandpaper (400 grit), then the sample was oxidized by exposure to air at ambient pressures for ~40 min. After introduction to the UHV, the oxidized sample underwent one set of Ar-ion treatment, where it was bombarded with Ar ions (1.7 kV/20 mA, $p \sim 1 \times 10^{-5}$ Torr in the chamber), typically for a period of 30 min, for multiple times and at nominal room temperature. The sample was not annealed. During these experiments, the XPS capability was unavailable, thus no XPS data were collected on this specific Ce sample. However, based upon previous experience, it is very likely that

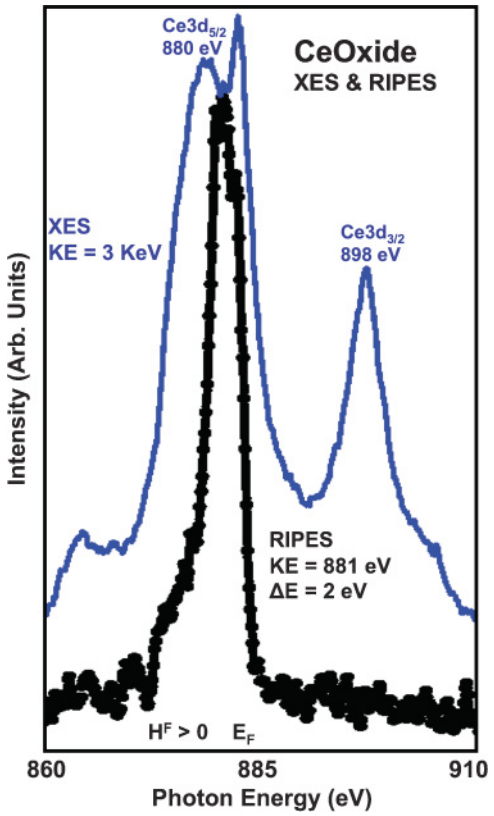

FIG. 1. (Color online) XES and RIPES of the Ce oxide.

the sample contained only Ce and O after sputtering with the Ar ions. Therefore, the assertion of cleanliness of the Ce oxide sample was indirectly supported by XPS. One set of XES measurements was performed as a test of sample composition and quality, as will be discussed below. Sample stability was addressed via the internal consistency of the sequential BIS and RIPES scans at different kinetic energies.

The XES and IPES and BIS spectra were collected using a Specs electron gun for the excitation and a XES 350 grating monochromator and channel-plate system from Scienta as the photon detection. Spectra were collected in "normal mode," where the electron gun KE and the energy position of the center of the channel plate were both fixed and the energy distribution in the photon ($h\nu$) spectrum was derived from the intensities distributed across the channel-plate detector in the energy dispersal direction. XES and RIPES data collection occurred with the sample at or near room temperature. In our experiments, the XES spectra play two critical roles: (1) the definition of the location of the resonance in energy space for RIPES and (2) the confirmation of the sample quality. Topic (2) will be discussed below. However, the definition of the absolute energy scale was made with IPES, as will be discussed next.

Energy scale calibration in PES and IPES is best performed by direct measurement of the location of the Fermi edge over a wide series of photon energies. As shown in Fig. 2, the underlying energy conservation relationship for IPES and BIS is when $h\nu + H^F$ is equal to KE + ϕ, where $h\nu$ is the photon energy, H^F is the energy of the empty state (hole) filled, relative to the Fermi energy (E_F), KE is the kinetic energy of the incoming electron, and ϕ is some sort of work function. Because the KE used here is from the output of the electron gun system, ϕ is a spectrometer work function and can contain contact potentials and other offsets. By looking at the Fermi edge, H^F is set to zero. Unfortunately for the Ce oxide, the only IPES observed was RIPES, at or near the resonance, as will be discussed below. However, by using the IPES of another material, UO_2, it was possible to observe Fermi edges over a wide range and thus calibrate the spectrometer exactly. Initial calibrations of the energy scale, based upon assigning the literature values[29] for the peaks at the Ce $M\alpha$ ($3d_{5/2}$) and

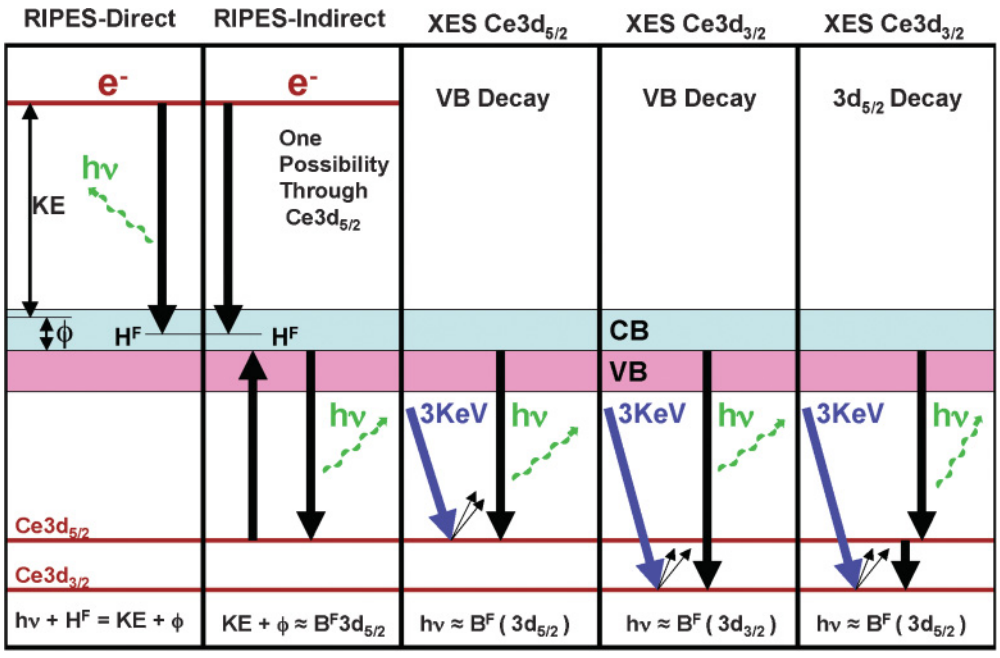

FIG. 2. (Color online) Schematic models for the processes of XES and RIPES.

$M\beta$ ($3d_{3/2}$) thresholds, lead to too large of a spectrometer work function. Using the UO_2 data and a type of linear regression analysis upon the data, a photon monochromator shift, $\Delta\lambda = 0.35$ Å, was determined, which then gave rise to an instrumental work function value of ~2 eV. (See KE = 881 eV in Fig. 1.) The same shift of $\Delta\lambda = 0.35$ was applied to the O 1*s* spectra, with the appropriate scaling with the photon energy squared.

Data collection was performed under UHV conditions. The base pressure of the system was 3×10^{-10} Torr, but the pressure changed depending on the energy and current of the electron gun. For example, with the XES measurements at KE = 3 keV, the pressure was ~8–9 $\times 10^{-10}$ Torr and the excitation current to the sample was typically 0.01 mA, but for RIPES at a KE of ~900 eV, it was ~5 $\times 10^{-10}$ Torr and 0.003 mA. XES data collection required many hours for each spectrum and RIPES spectra took substantially longer.

As will be discussed below, our sample consisted of a thin layer of Ce oxide lying above Ce metal. Under conditions such as these, thin layers composed of materials that would normally be insulating in the bulk can continue to exhibit a Fermi edge, owing to the thinness of the film and the underlying conductor.[30] It is for this reason that we will refer to the sample as a Ce oxide. Although thermodynamic arguments under oxidizing conditions point to CeO_2, it can be argued that "tetravalent" CeO_2 is unstable and not obtained under these preparation conditions, but only by annealing the sample in an O_2 atmosphere. It is very likely that our Ar-ion treatment drove the sample into a stable configuration dominated by Ce_2O_3, as reported earlier by Allen.[7] Below, spectroscopic evidence will be presented to support this hypothesis. Next, energy bandpass and broadening effects will be considered.

In general, the observed energy widths in the RIPES and XES experiments follow (1):

$$\Delta E_{\text{total}} = [(\Delta E_{\text{ex}})^2 + (\Delta E_{\text{det}})^2 + (\Delta E_{\text{life}})^2 + (\Delta E_{\text{chem/mult}})^2]^{1/2}. \quad (1)$$

Here, ΔE_{ex} is the energy broadening from the excitation source, the electron gun. ΔE_{det} is the broadening from the photon detection, i.e., the monochromator and the multichannel detection of the XES. ΔE_{life} is the intrinsic broadening owing to lifetime and other such effects and $\Delta E_{\text{chem/mult}}$ would be the broadening from the presence of different chemical sites or an underlying multiplet structure.

Let us first consider the case of the RIPES experiments, using Fig. 1 as a guide. In Fig. 1, there is a fairly sharp Fermi edge just below $h\nu = 885$ eV. The 10%–90% width of a Fermi edge provides a direct measure of the total energy broadening, ΔE_{total}. Our measurements indicate that $\Delta E_{\text{total}} = 2$ eV, regardless of whether the monochromator entrance slit width was 20 or 60 μm. For our monochromator system, it is known that the energy broadening from the photon detection, ΔE_{det}, should be 0.35 eV for a 20-μm slit width and 1.1 eV for a 60-μm slit width. It is also well known that the intrinsic room-temperature width of a Fermi edge is on the scale of 0.1 eV. Finally, as will be discussed below, this Fermi edge lines up with the higher-energy peak in the Ce $3d_{5/2}$ XES manifold, indicating that it arises solely from oxide and not metallic Ce. This suggests that here $\Delta E_{\text{chem/mult}} \cong 0$ eV. Taken together, this indicates the following for the RIPES experiments.

$$\Delta E_{\text{total}}^{\text{RIPES}} = \Delta E_{\text{ex}}^{\text{RIPES}} = 2 \text{ eV}. \quad (2)$$

Despite the apparent lack of dependence upon slit size, for some measurements slit sizes were varied, as a test of data set consistency. It is also useful to note that the RIPES spectra exhibit a Fermi edge that is substantially sharper than any features in the XES spectra, as can be seen in Fig. 1.

Now, let us consider the XES experiments, again using Fig. 1 as a guide. As can be seen easily in the Ce $3d_{3/2}$ peak, $\Delta E_{\text{total}}^{\text{XES-3/2}} \approx 4$ eV, based upon the full width at half max (FWHM) of the Ce $3d_{3/2}$ peak. Here, $\Delta E_{\text{ex}} = 0$ eV, because, at energies well above the threshold, the excitation energy width used to generate the initial core hole does not affect the decay event energetics. From the RIPES energy analysis above, it is known that $\Delta E_{\text{det}} \leqslant 1$ eV. This suggests the following, for the XES-3/2 experiment:

$$\Delta E_{\text{total}}^{\text{XES-3/2}} = \left[\left(\Delta E_{\text{life}}^{\text{XES-3/2}}\right)^2 + \left(\Delta E_{\text{chem/mult}}^{\text{XES-3/2}}\right)^2\right]^{1/2} \approx 4 \text{ eV}. \quad (3)$$

For the XES-5/2 experiment, it is less clear, so a more general equation is required. The impact of these equations will be discussed below:

$$\Delta E_{\text{total}}^{\text{XES-5/2}} = \left[\left(\Delta E_{\text{det}}^{\text{XES-5/2}}\right)^2 + \left(\Delta E_{\text{life}}^{\text{XES-5/2}}\right)^2 + \left(\Delta E_{\text{chem/mult}}^{\text{XES-5/2}}\right)^2\right]^{1/2}. \quad (4)$$

III. SPECTRAL RESULTS AND DISCUSSION

A. Resonance processes

Consider the individual excitation and decay channels for nonresonant XES, IPES, and RIPES, shown below in Eqs. (5)–(8). The Ce-derived valence bands (VBs) will include both the 4*f* and *spd* states, where the *spd* states are derived from the 6*s*, 6*p*, and 5*d* states. The Ce-derived conduction bands (CBs), normally empty, will have a 4*f* character as well as an *spd* character. To begin our discussion, let us define the initial-state electronic configuration as follows: VB^nCB^0 with $n \leqslant 4$. The different cases discussed below are also schematically illustrated in Fig. 2.

(1) Off-resonance XES: High-energy excitation and decay:

$$e^- + 3d^{10}VB^n \rightarrow 3d^9VB^n + 2e^-, \quad (5a)$$

$$3d^9VB^n \rightarrow 3d^{10}VB^{n-1} + h\nu. \quad (5b)$$

(2) On-resonance XES: Excitation and decay at the threshold:

$$e^- + 3d^{10}VB^n \rightarrow 3d^9VB^{n+2} \rightarrow 3d^{10}VB^{n+1} + h\nu. \quad (6)$$

(3) Off-resonance IPES and RIPES direct channel:

$$e^- + 3d^{10}VB^n \rightarrow 3d^{10}VB^{n+1} + h\nu. \quad (7)$$

(4) RIPES indirect channel:

$$e^- + 3d^{10}VB^n \rightarrow 3d^9VB^{n+2} \rightarrow 3d^{10}VB^{n+1} + h\nu. \quad (8)$$

It is appropriate to begin with XES. When the incoming excitation is at high energies, substantially above the core-level

binding energy of the 3*d* levels, then it is expected that the Ce atom will lose a single electron, with a +1 change in net charge, with both the excitation electron and 3*d* core-level electron leaving the atom. For example, this occurs when the excitation energy is 3 or 1.5 keV and the core-level binding energy is near 900 eV. The appropriate relations for this case are shown in Eq. (5). However, as the excitation energy is decreased, until it is just above threshold, a different regime is encountered. Here, the excitation electron has only enough energy to lift the 3*d* core-level electron into the previously empty CBs, with itself also in the CBs. The Ce atom has gained an electron, with the net charge on the atom decreased by −1. Very quickly, a decay process can occur, giving rise to the filling of the 3*d* core hole and the emission of an electron, with a net increase of the occupancy of the VBs by 1, with a retention of the net charge change of −1. This situation is illustrated in Eq. (6). In both limits, the photon emitted in the decay processes, shown in Eqs. (5b) and (6), will have an energy near that of the 3*d* core level, adjusted for effects such as screening, relaxation, and charge.

In IPES, the situation is as follows. Off-resonance or regular IPES involves an electron dropping into the CB and the emission of a photon. The net charge decreases, by −1, with the emission of a photon, as summarized in Eq. (7). The photon is emitted with an energy that roughly corresponds to the energy of the incoming electron, as shown in Fig. 2. (ϕ and H^F are both small.)

Finally, the case of RIPES is considered here. In RIPES, there are two channels, referred to as direct and indirect. The direct channel, in Eq. (7), is the same as the lone channel of off-resonance IPES. The indirect channel, shown in Eq. (8), is the same as the near-threshold XES of Eq. (6). Here, the final state will have a net decrease in charge of −1, associated with the increase of electron occupancy by 1. The emitted photon energy, 3*d* core-level energy, and incoming electron excitation energy must all be approximately equal, as shown in Fig. 2.

In the present study, the process of resonant inverse photoemission is being invoked to explain the experimental observations. However, the corresponding resonant process in the photoemission of Ce has been studied for many years. In fact, resonant photoelectron spectroscopy (RES-PES) at the Ce 4*d* and 3*d* thresholds was performed decades ago by Allen,[7] Laubschat *et al.*,[31] and Suga's group.[32] Here, the interference of the direct photoemission channel and an indirect channel, using a *d*-4*f* dipole excitation followed by a decay that ends up in the same final state as the direct process, can give rise to an interference that leads on resonance to a strong enhancement of the Ce 4*f* emission. In this study, the inverse process is considered, specifically the interference of the direct IPES direct channel and an IPES indirect channel, driven by an electron-induced 3*d* excitation and followed by a dipole transition. As in the case of the PES process resonance, the IPES process resonance will hinge upon the *f*-*d* dipolar transition. The indirect IPES channel will be dominated by a 4*f*-to-3*d* transition, following electric dipole selection rules and generating the emission of a photon. Similarly, it is reasonable to expect that the excitation will be dominated by 3*d*-to-4*f* transitions, driven by the large density of empty 4*f* states and their spatial localization close to the 3*d* orbitals, despite the lessened selectivity of the Coulombic matrix elements associated with excitation by kilovolt range electrons. Thus, the key to resonance is the *d*-*f* dipolar transitions.

Now, let us return to a consideration of the nature of the Ce oxide VBs and CBs. In metallic Ce, something such as $4f^1(spd)^3\mathrm{CB}^0$ would be expected, reflecting the notion that Ce metal is "trivalent." If the Ce oxide were CeO_2 and were completely ionized, then $4f^0(spd)^0\mathrm{CB}^0$ would be expected. This is the so-called "formal charge," which assumes complete success by the oxidizing agent in the ionization process. If the Ce oxide were Ce_2O_3 and were completely ionized, again a "formal charge," then $4f^{1-x}(spd)^x\,\mathrm{CB}^0$ would be expected, with x near or at zero. However, the Ce oxide is probably only partially oxidized and partially ionized, with a possible component of covalency and partial occupation. Thus, whether the Ce oxide is either CeO_2 or Ce_2O_3, it is not unreasonable to expect the Ce VBs and CBs to be something such as $4f^{1-a}(spd)^{3-b}\,\mathrm{CB}^0$, with $0 \leqslant a \leqslant 1$ and $0 \leqslant b \leqslant 3$ and $a + b \leqslant 4$ for CeO_2 and $a + b \leqslant 3$ for Ce_2O_3. It is also reasonable to expect the *spd* states to ionize more easily that the 4*f* states. Hence, one would expect the following: $3 - b < 1 - a$. In any case, there will be no shortage of unoccupied 4*f* states for the excitation process: There will be a minimum of 13 and a maximum of 14. However, while it is possible that the 4*f* electron generated by the excitation will also participate in the decay, any additional original occupation of the Ce 4*f* states would probably strongly enhance the decay process. Thus, the observation of a resonant effect in the RIPES of the Ce oxide strongly favors the assignment of the Ce oxide as Ce_2O_3, and not CeO_2. Lastly, the interpretation of the resonance as arising from Ce_2O_3 is consistent with the earlier observations by Allen of a strong 4*d* RES-PES effect in Ce_2O_3.[7]

B. Confirmation of sample quality

XES of the Ce $3d_{5/2}$, Ce $3d_{3/2}$, and O 1*s* levels was used to characterize the Ce oxide sample. As shown in Fig. 1, there are two components to the $M\alpha$ ($3d_{5/2}$) peak but only one for the $M\beta$ ($3d_{3/2}$) peak. This is not surprising: The larger lifetime broadening associated with the $M\beta$ ($3d_{3/2}$) threshold can smear out fine structure. Some of the processes involved in the production of these spectral features can be seen in Fig. 2. Because $3d_{3/2}$ states are at a higher binding energy relative to the Fermi level (B^F) than the $3d_{5/2}$ states, a fast, nonradiative decay through the $3d_{5/2}$ states is possible, contributing to the broadening. Furthermore, decay channels such as this can also explain the divergence of the peak intensities from the "statistical" limit, where intensity should scale with the number of states. In this limit, the ratio of the intensities, $3d_{5/2}$ vs $3d_{3/2}$, should be 3 : 2. The observed intensity ratio is quite a bit larger, as can be seen in Fig. 1. Next, we will use the KE dependence of the excitation to probe the origin of the splitting in the $3d_{5/2}$ peak and relate that to the sample structure.

As shown in Fig. 3, it is possible to induce changes in the relative intensities of the two components in the Ce $3d_{5/2}$ spectral feature. These two components will be assigned to the underlying Ce metal and the near-surface Ce oxide thin film. There are two data sets shown in Fig. 3, corresponding to two different slit sizes for the monochromator. Temporally, these four spectra were taken one after the other, contiguously.

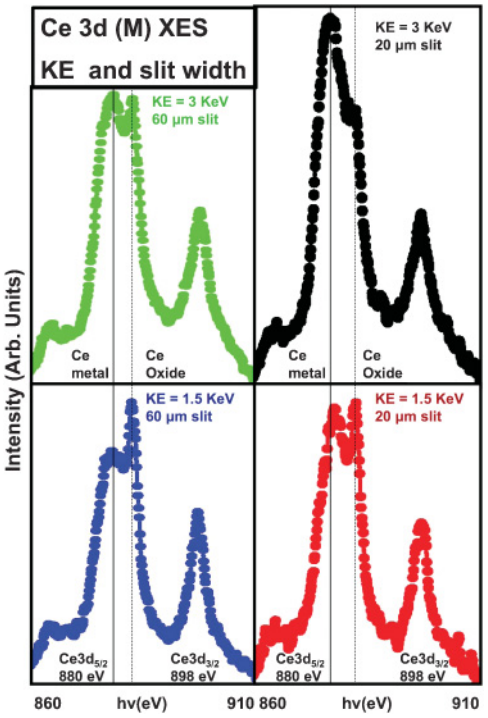

FIG. 3. (Color online) Plots of the XES of the Ce 3*d* states, including their dependences upon KE and the monochromator entrance slit width. The spectra were normalized to the Ce $3d_{3/2}$ peak heights. See text for details.

In both cases, lowering the KE from 3 to 1.5 keV enhances the second component of the Ce $3d_{5/2}$ spectral feature. Under these conditions, the escape depths of the photons should not be a factor, but the penetration depths of the electrons should. By lowering the KE, the surface sensitivity is increased. This argues for the material associated with the subpeak at the lower photon energy to be underneath the material associated with the subpeak at the higher photon energy. It is reasonable to assume that the underlying material is metallic Ce and that the layer above it is oxidized Ce. This assignment is confirmed by a consideration of the literature and previous experiments. It was shown earlier by Baer and co-workers[6] that CeO_2 exhibited additional spectral structures in XPS and EELS at higher binding energies, relative to Ce metal. This result has been confirmed by others, using XPS (Ref. 18) and EELS.[22] Similar intensity shifts to higher energies has been observed in XAS as well.[19] In fact, as part of a previous collaboration,[20] we have observed this shift before, utilizing XAS on Beamline 8 at the Advanced Light Source.[21] Using oxidized bulk Ce samples, it was possible to see a strong, shifted spectral structure that could be removed by scraping, giving rise to a final XAS result that approximated the evaporated samples utilized in our other study.[20] Thus, there is very strong evidence to support the assignment of the lower photon energy subpeak in the Ce $3d_{5/2}$ manifold to the underlying bulk metallic Ce and the higher photon energy subpeak to a near-surface layer of the Ce oxide. Additionally, it should be noted that there appears to be a very weak enhancement of a low *hv* shoulder on the Ce $3d_{3/2}$ peak, as the KE is increased from 1.5 to 3 keV. This lower *hv* shoulder would correspond to the Ce metal Ce $3d_{3/2}$ contribution. However, the enhancement of the shoulder in the Ce $3d_{3/2}$ peak is very weak and should be regarded with caution. The larger lifetime broadening expected for the lower *j* component of the spin-orbit split doublet appears to smear out any underlying fine structure.

Now, let us consider the changes in peak shape as a function of slit width. In both cases, for KE = 1.5 keV and KE = 3.0 keV, in going from a slit width of 20–60 μm, the peak height of the Ce metal $3d_{5/2}$ peak increases noticeably, with a corresponding change in peak shape. The rest of the spectra remain essentially the same: the Ce $3d_{3/2}$ peak and the Ce oxide $3d_{5/2}$ subpeak. We believe these observations are a function of the interplay of lifetime broadening and the monochromator energy resolution bandpass. Consider Eq. (3) above. For the Ce $3d_{3/2}$ peak, we concluded that the peak width was driven by lifetime broadening and underlying structure owing to chemical shifts and a multiplet structure. However, we also note above that the high *hv* shoulder in the Ce $3d_{3/2}$ peak is very weak. Furthermore, the triangular peak shape is consistent with the Lorentzian function associated with lifetime broadening. Thus, the energy width in the Ce $3d_{3/2}$ peak is dominated by lifetime effects. This result is shown in Eq. (9):

$$\Delta E_{\text{total}}^{\text{XES-3/2}} = \left(\Delta E_{\text{life}}^{\text{XES-3/2}}\right) \approx 4 \text{ eV}. \tag{9}$$

Equation (9) implies that the Ce $3d_{3/2}$ peak should be independent of the slit width. The spectra in Fig. 3 are consistent with this assertion. Thus, it is justified to use the height of the Ce $3d_{3/2}$ peak as a type of normalization.

Next, the subpeaks in the Ce $3d_{5/2}$ peak will be considered. Because the two subpeaks overlap, the analysis will need to couched in terms of the half widths at half maximum (HWHM), using the outside halves of each subpeak for the analysis. Also, because the subpeaks are being separated upon the basis of their chemical origin, it will be assumes that the $\Delta E_{\text{chem/mult}}$ can be neglected. For the case of the Ce oxide Ce $3d_{5/2}$ peak, it can be seen that the peak is essentially constant, regardless of slit width and KE, relative to the Ce $3d_{3/2}$ peak. The peak height remains fairly uniform and the triangular and Lorentzian peak shape is robustly retained, with a HWHM also on the same scale as that of the Ce $3d_{3/2}$ peak. This strongly suggests that the Ce oxide Ce $3d_{5/2}$ peak is also dominated by lifetime effects, with no dependence up the any internal structure or the monochromator resolution:

$$\Delta E_{\text{total-Ce oxide}}^{\text{XES-5/2}} = \Delta E_{\text{life-Ce oxide}}^{\text{XES-5/2}}. \tag{10}$$

Interestingly, both the XAS work by Kaindl *et al.*[19] and our unpublished work[20,21] suggest that the Ce oxide Ce $3d_{5/2}$ peak has a line shape and linewidth quite similar to that of the Ce oxide Ce $3d_{3/2}$ peak, while the Ce metal Ce $3d_{5/2}$ peak has a more internal fine structure and a more sharply rising line shape than the corresponding Ce metal Ce $3d_{3/2}$ peak. This would be consistent with a lifetime broadening limit in the Ce oxide Ce $3d_{5/2}$ peak but a possible dependence upon both lifetime broadening and instrumental broadening in the Ce metal Ce $3d_{5/2}$ peak. Thus, for the Ce metal Ce $3d_{5/2}$ peak, the following is appropriate:

$$\Delta E_{\text{total-Ce metal}}^{\text{XES-5/2}} = \left[\left(\Delta E_{\text{det}}^{\text{XES-5/2}}\right)^2 + \left(\Delta E_{\text{life-Ce metal}}^{\text{XES-5/2}}\right)^2\right]^{1/2}. \tag{11}$$

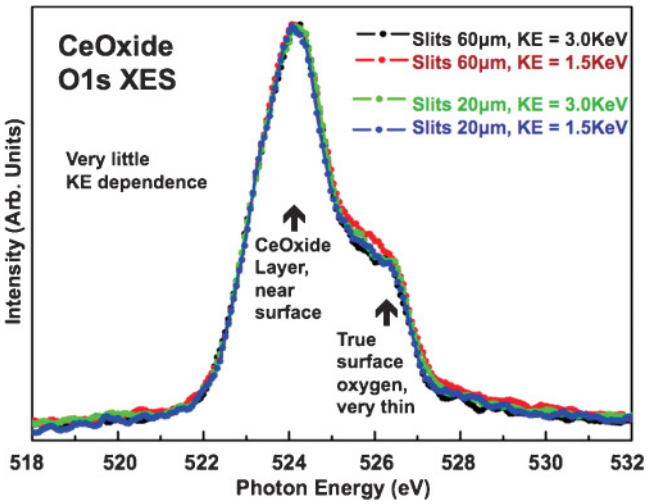

FIG. 4. (Color online) XES of the O 1*s*.

From Eq. (11), a lifetime broadening of ∼1–2 eV can be obtained. This has been done using: (1) a simple line-shape model that assumes an inverse proportionality between peak height and peak width, for constant peak area; (2) the experimentally observed peak height increase of $\sim\frac{1}{4}$ between the 20- and 60-μm spectra of Fig. 3; and (3) the values of $\Delta E_{\rm det}(20\ \mu{\rm m}) \approx 0.35$ eV and $\Delta E_{\rm det}(60\ \mu{\rm m}) \approx 1.1$ eV. This result is shown in Eq. (12):

$$1\ {\rm eV} \leqslant \Delta E^{\rm XES\text{-}5/2}_{\rm life\text{-}Ce\ metal} \leqslant 2\ {\rm eV}. \qquad (12)$$

The total linewidths from this model would be on the scale of 2–3eV, in accord with the spectra in Fig. 3. This result in Eq. (12) is consistent with the earlier XAS results and explains the increase in the peak height of the Ce metal Ce $3d_{5/2}$ peak relative to the other constant spectral features.

The above interpretation is further supported by the O 1*s* XES data plotted in Fig. 4. First, there can be no doubt that this sample is an oxide of some sort: A strong O 1*s* spectral feature is clearly evident. Second, the result is independent of electron excitation energy, for both data sets with different slit sizes, indicating that all of the oxygen is at or near the surface, not in the bulk. Third, most of the intensity is in the main feature at a photon energy of 524 eV. This main feature is assigned to the near-surface thin film of Ce oxide. The second, smaller feature near 526 eV, is associated with true surface oxygen, possibly physically or chemically attached to the top of the Ce oxide layer. It is reasonable to expect that the physically or chemically attached oxygen may be in a higher oxidation state, i.e., without the oxidized electrons from Ce, and would thus be at a higher photon energy. (Because oxygen is the oxidizing agent, it is the Ce that gets oxidized and the oxygen that gets reduced. A reduced atom may have less of a tight hold upon its electrons, thus giving rise to a lower binding energy. Hence, the oxygen in the Ce oxide is expected to have a lower O 1*s* binding energy than the physically or chemically absorbed oxygen species.)

Thus, supported by the XES results, our picture is the following. The bulk Ce is coated with a thin film of Ce oxide, but thin enough that we see the retention of a Fermi edge in the RIPES spectra.

Finally, before going on to a discussion of the RIPES results, there is one last feature to discuss in the XES spectra in Figs. 1 and 3. In the XES spectra there are also weak features near 865 and 905 eV. Because our data collection is performed in normal mode, it is possible that weak features such as these are artifacts of the monochromator and/or channel-plate signature. Because of their weakness, a further analysis was not pursued. Next, the RIPES spectra will be described and discussed.

C. RIPES of the Ce 3*d* states

A strong resonance in the RIPES of the Ce oxide has been observed. Here, we will present the experimental XES and RIPES data and discuss them within the framework of previous results.

As shown in Fig. 1, the RIPES and XES are coincident in energy space. This coincidence is independent of any energy-scale calibration, because the same monochromator settings were used in each data collection. Only the energy of the incoming excitation electrons was changed. The difference in the spectra is owing to the change in the energy of the incoming beam. For the XES, the excitation beam is at an energy of 3 keV, well above the Ce $M\alpha$ ($3d_{5/2}$) and $M\beta$ ($3d_{3/2}$) thresholds. As illustrated in Fig. 2, the electron beam serves only to scatter off of the core-level electrons and generate a core hole, beginning the process that ultimately gives rise to the photon emission at the characteristic energies associate with XES. Using the XES as a guide, a photon energy window was thus chosen for the RIPES experiments. As can be seen in Fig. 1, the RIPES spectrum at KE = 881 eV is much sharper than the XES spectrum. Consistent with the picture shown in Fig. 2, there is no intensity at the higher photon energies, above E_F. This is because the transitions in this regime would correspond to the incoming electron dropping into an occupied state, which is forbidden. The intensity jump occurs at E_F and continues into the regime where H^F is greater than zero, where the incoming electron is dropping into the unoccupied conduction band. The defining characteristic of IPES is that KE $\approx h\nu$. For RIPES to occur, a second, indirect channel must open up, providing an additional path into the final state associated with IPES. There are further, quantum-mechanically-driven aspects to a resonance, but that discussion can be found elsewhere.[7,31–33] Energetically, the defining characteristic of being on resonance is that KE $\approx B^F$, the core-level binding energy relative to the Fermi level, E_F. Thus for RIPES, $h\nu \approx$ KE $\approx B^F$, as presented schematically in Fig. 2. As the photon energy is diminished further, the RIPES intensity drops, with the final state moving out of the higher-density CBs and into the less dense, more-free-electron-like states.

Spectral summaries of the RIPES and XES are shown in Figs. 5 and 6 for the Ce $3d_{5/2}$ and Ce $3d_{3/2}$ thresholds. In both cases, it is clear that the resonance occurs only within the confines of the energy regime defined by the XES spectrum. Each time, the resonance begins to turn on as the excitation KE approaches the photon energy associated with the XES peak. The maxima are obtained when the KE reaches an approximate equivalence with the photon energy associated with the corresponding XES peak. As mentioned before, in the Ce $3d_{5/2}$ regime, the resonance is associated with only the

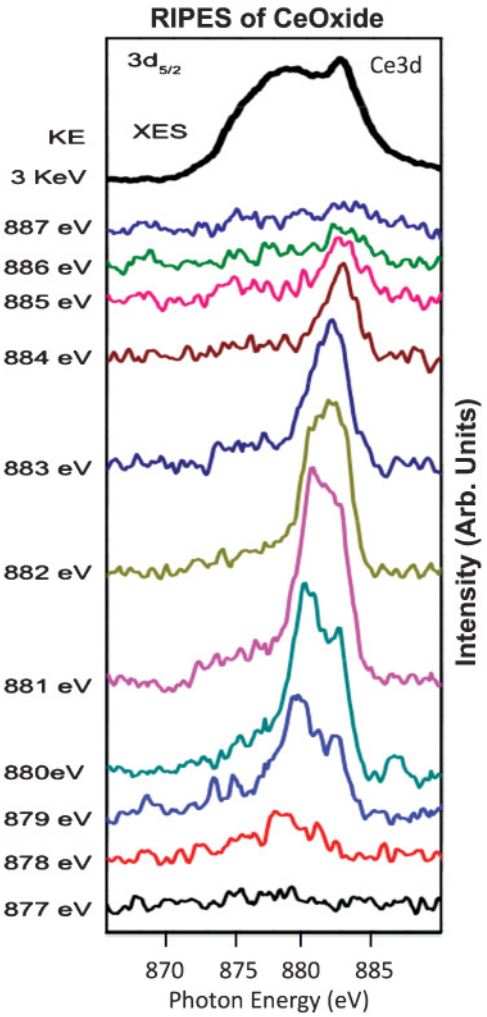

FIG. 5. (Color online) A plot of both the XES and RIPES near the Ce $3d_{5/2}$ threshold, including the photon energy dependence of the Ce $3d_{5/2}$ RIPES resonance.

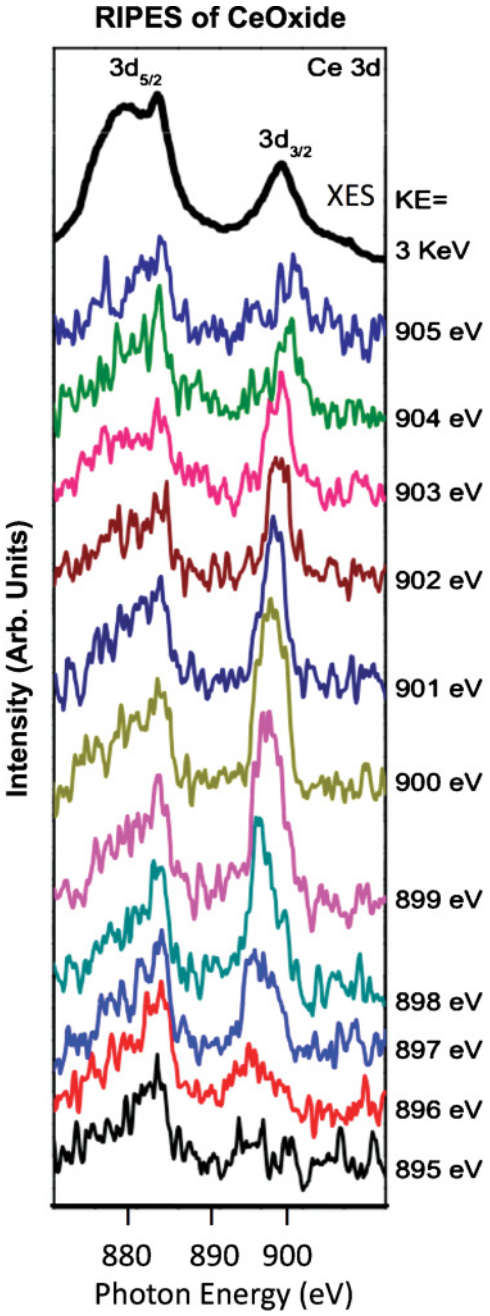

FIG. 6. (Color online) A plot of both the XES and RIPES near the Ce $3d_{3/2}$ threshold, including the photon energy dependence of the Ce $3d_{3/2}$ RIPES resonance.

Ce oxide XES peak, not the Ce metal XES peak at lower photon energies. In the case of the Ce $3d_{3/2}$ regime, the separation of the metal and oxide contributions is lost, presumably owing to the increased lifetime broadening of the 3/2 feature.

It is of interest to look carefully at the photon energy dependence of the IPES. For the Ce $3d_{5/2}$, there appear to be weak intensities at KE = 877, 878, 886, and 887 eV, which suggest off-resonance spectral structure, shifting with KE. This would be the spectral dispersion of the IPES Fermi edge, driven by the linear relationship between $h\nu$ and KE, as shown in Fig. 2. In the intervening KEs, the resonance is dominant and the intensity reflects not so much the Fermi edge dispersion with the changing KE but instead the onset and subsequent diminishment of a peak with a fixed high-energy cutoff, as it moves through resonance with a maximum at KE = 881 eV. In the regime of KE = 879–885 eV in Fig. 5, it is clear that the leading edge of the peak does not move. This leading edge is the Fermi edge at the resonant energy, KE = 881 eV, which is directly below the peak in the Ce oxide XES feature, as shown in Figs. 1 and 5. At lower KEs, 879–881 eV, the width of the main feature diminishes with increasing KE. This suggests that a regular IPES peak is walking up to the resonance and then becoming energy coincident and integrally part of the resonance at 881 eV. At energies above the resonance, 883–885 eV, the width of the spectra feature again diminishes, suggesting that the resonance is persisting as the tail of the IPES peak but with a cutoff corresponding to the KE = 881 eV Fermi edge. Finally, at KE = 886 and 887 eV, there may actually be a shift in the Fermi edge position with increasing KE, although with much weaker intensity. A similar process occurs for the Ce $3d_{3/2}$ resonance, with a maximum of the higher photon energy peak occurring at KE near 900 eV. Again, in the regime of KE = 897–903 eV, as the main peak walks up in photon energy and the resonance occurs, the peak

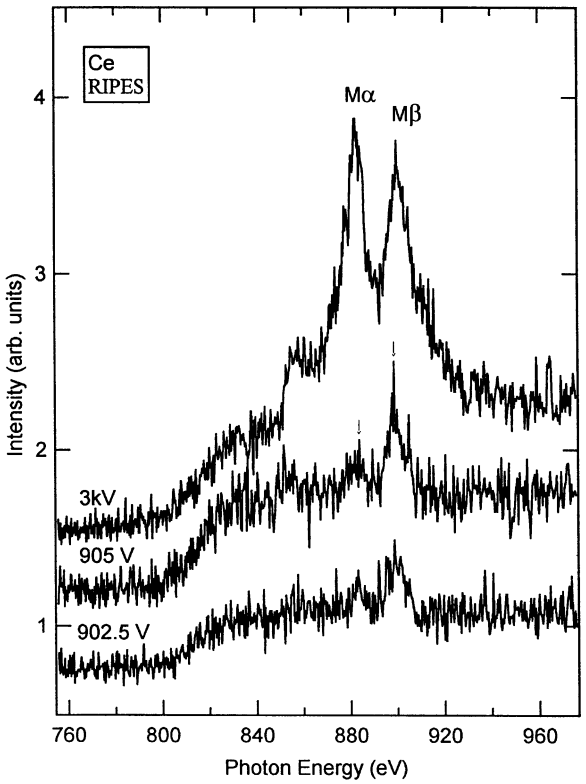

FIG. 7. The RIPES and XES of the Ce metal (Refs. 34 and 35).

width narrows as the peak position moves toward the cutoff at the Fermi edge associated with the resonance maximum at KE = 900 eV. The Ce $3d_{3/2}$ RIPES is complicated by the presence of a Ce $3d_{5/2}$ peak. This is the RIPES manifestation of the nonradiative decay process shown in Fig. 2. Thus, some of the Ce $3d_{3/2}$ RIPES intensity is lost to this XES-like feature. It is interesting that at the KEs below the threshold for resonance in the Ce $3d_{3/2}$ regime, e.g., KE = 895 and 896 eV, the XES-like feature associated with the Ce $3d_{5/2}$ energy dominates the spectra. As the Ce $3d_{3/2}$ resonance turns on, the feature at the Ce $3d_{3/2}$ energy becomes dominant, but the Ce $3d_{5/2}$ peak persists. Above the resonance, at KE = 905 eV, the envelope of the spectrum becomes similar to that observed at much higher excitation energies, i.e., KE = 1.5 and 3 keV. (Fig. 3) Again, there is some evidence of weak dispersion of the Fermi edge, at kinetic energies below (KE = 895 and 896 eV) and above (KE = 904 and 905 eV) the resonant regime.

As described above, the resonance is associated with the Ce oxide and not the metallic Ce. This interpretation is confirmed by a consideration of the spectra shown in Fig. 7. Here, the results of measurements of metallic Ce, carried out in a similar spectrometer, are presented.[34,35] The resonance appears to be far weaker in the metallic Ce than in the Ce oxide. The picture of resonance enhancement with the transition from delocalized to localized behavior is not new, and this interpretation is consistent with a picture put forward earlier by Dowben.[36] In Dowben's picture, delocalization serves to provide alternate, interatomic decay channels that tend to subtract from the resonant enhancement. Localization maximizes the resonance by restricting access to these additional channels, instead optimizing the decay via the indirect, intra-atomic channel (Fig. 2) that is energy coincident with the IPES direct channel.

Finally, it is useful to compare our results to those of Liefeld, Burr, and Chamberlain.[9] Our RIPES spectroscopic results essentially are in complete agreement with theirs. The photon energy dependences at both the Ce $M\alpha$ ($3d_{5/2}$) and $M\beta$ ($3d_{3/2}$) thresholds are the same. Thus it seems very unlikely that the source of their RIPES was Ce metal, but rather is some sort of oxidized Ce, although the exact nature of the oxidation, either cerium oxide or cerium fluoride, remains unknown.

IV. SUMMARY AND CONCLUSIONS

Strong resonant behavior in the IPES of a thin layer of Ce oxide, near the Ce 3*d* edges, has been observed. It confirms the picture of resonance enhancement with localization and explains the observations of Liefeld, Burr and Chamberlain from 35 years ago.

ACKNOWLEDGMENTS

Lawrence Livermore National Laboratory is operated by Lawrence Livermore National Security, LLC, for the US Department of Energy, National Nuclear Security Administration under Contract No. DE-AC52–07NA27344. This work was supported by the DOE Office of Science, Office of Basic Energy Science, Division of Materials Science and Engineering. We would like to thank Emiliana Damian-Risberg for her work on the experiments in Sweden, Jonathan Denlinger for his help with the Beamline 8 experiments at the ALS and Thorsten Schmitt and Jinghua Guo for their mentoring of E.D.-R.

*Tobin1@LLNL.Gov

[1]G. Denninger, V. Dose, and H. P. Bonzel, Phys. Rev. Lett. **48**, 279 (1982); V. Dose, Appl. Phys. **14**, 117 (1977).

[2]P. D. Johnson and N. V. Smith, Phys. Rev. Lett. **49**, 290 (1982).

[3]F. J. Himpsel and Th. Fauster, Phys. Rev. Lett. **49**, 1583 (1982).

[4]B. J. Knapp and J. G. Tobin, Phys. Rev. B **37**, 8656 (1988).

[5]J. G. Tobin, Photoemission and Inverse Photoemission, in *Determination of Optical Properties*, Vol. VIII of *Physical Methods of Chemistry*, 2nd ed., edited by B. W. Rossiter and R. C. Bretzold (John Wiley and Sons, New York, 1993), and references therein.

[6]E. Wuilloud, B. Delley, W. D. Schneider, and Y. Baer, Phys. Rev. Lett. **53**, 202 (1984); E. Wuilloud, H. R. Moser, W. D. Schneider, and Y. Baer, Phys. Rev. B **28**, 7354 (1983).

[7]J. W. Allen, J. Magn. Mater. **47/48**, 168 (1985); J. Less-Common Met. **93**, 183 (1983).

[8]P. Kuiper, J. van Elp, G. A. Sawatzky, A. Fujimori, S. Hosoya, and D. M. de Leeuw, Phys. Rev. B **44**, 4570 (1991).

[9]R. J. Liefeld, A. F. Burr, and M. B. Chamberlian, Phys. Rev. A **9**, 316 (1974); M. B. Chamberlain, A. F. Burr, and R. J. Liefeld, *ibid.* **9**, 663(1974).
[10]F. Reihle, Phys. Status Solidi **98**, 245 (1980).
[11]Y. Hu, T. J. Wagener, Y. Gao, and J. H. Weaver, Phys. Rev. B **38**, 12708 (1988).
[12]P. Weibel, M. Grioni, D. Malterre, B. Dardel, and Y. Baer, Phys. Rev. Lett. **72**, 1252 (1994); M. Grioni, P. Weibel, D. Malterre, Y. Baer, and L. Du'o, Phys. Rev. B **55**, 2056 (1997).
[13]B. E. Mason and R. J. Liefeld, J. Vac. Sci. Technol. A **8**, 4057 (1990).
[14]D. Wieliczka, J. H. Weaver, D. W. Lynch, and C. G. Olson, Phys. Rev. B **26**, 7056 (1982)
[15]E. Vescovo and C. Carbone, Phys. Rev. B **53**, 4142 (1996).
[16]E. Weschke, C. Laubschat, T. Simmons, M. Domke, O. Strebel, and G. Kaindl, Phys. Rev. B **44**, 8304 (1991).
[17]P. Patsalas, S. Logothetidis, L. Sygellou, and S. Kennou, Phys. Rev. B **68**, 035104 (2003).
[18]N. A. Braaten, J. K. Grepstad, and S. Raaen, Phys. Rev. B **40**, 7969 (1989).
[19]A. G. Kaindl, G. Kalkowski, W. D. Brewer, E. V. Sampathkumaran, F. Holtzberg, A. Schach, and V. Wittenau, J. Magn. Magn. Mater. **47/48**, 181 (1985); B. C. Bonnelle, R. C. Karnatak, and J. Sugar, Phys. Rev. A **9**, 1920 (1974).
[20]K. T. Moore, B. W. Chung, A. J. Schwartz, J. G. Tobin, S. Lazar, F. D. Tichelaar, H. W. Zandbergen, P. Söderlind, and G. van der Laan, Phys. Rev. B **69**, 193104 (2004).
[21]J. D. Denlinger, Advanced Light Source, Lawrence Berkeley National Laboratory, Berkeley, CA, USA (private communication, 2003).
[22]J. Bloch, N. Shamir, M. H. Mintz, and U. Atzmony, Phys. Rev. B **30**, 2462 (1984).
[23]Lijun Wu, H. J. Wiesmann, A. R. Moodenbaugh, R. F. Klie, Yimei Zhu, D. O. Welch, and M. Suenaga, Phys. Rev. B **69**, 125415 (2004).
[24]C. Dallera, M. Grioni, A. Palenzona, M. Taguchi, E. Annese, G. Ghiringhelli, A. Tagliaferri, N. B. Brookes, Th. Neisius, and L. Braicovich, Phys. Rev. B **70**, 085112 (2004).
[25]M. Watanabe, Y. Harada, M. Nakazawa, Y. Oshiwata, R. Eguchi, T. Takeuchi, A. Kotani, and S. Shin, Surf. Rev. Lett. **9**, 983 (2002).
[26]J. G. Tobin, S. W. Yu, T. Komesu, B. W. Chung, S. A. Morton, and G. D. Waddill, Mater. Res. Soc. Symp. Proc. **986**, 63 (2007).
[27]S. W. Yu and J. G. Tobin, Phys. Rev. B **77**, 193409 (2008); Surf. Sci. Lett. **601**, L127 (2007).
[28]J. G. Tobin, S.-W. Yu, B. W. Chung, G. D. Waddill, and A. L. Kutepov, IOP Conf. Ser.: Mater. Sci. Eng. **9**, 012054 (2010).
[29]A. Thompson *et al.*, *X-Ray Data Handbook* (LBNL, Berkeley, CA, 2001).
[30]B. W. Veal and D. J. Lam, Phys. Rev. B **10**, 4902 (1974); Phys. Lett. A **49**, 466 (1974).
[31]C. Laubschat, E. Weschke, G. Kalkowski, and G. Kaindl, Phys. Scr. **41**, 124 (1990); C. Laubschat, E. Weschke, C. Holtz, M. Domke, O. Strebel, and G. Kaindl, Phys. Rev. Lett. **65**, 1639 (1990).
[32]R.-J. Jung, Byung-Hee Choi, S.-J. Oh, Hyeong-Do Kim, En-Jin Cho, T. Iwasaki, A. Sekiyama, S. Imada, S. Suga, and J.-G. Park, Phys. Rev. Lett. **91**, 157601 (2003); S.-J. Oh *et al.*, Solid State Commun. **82**, 581 (1992).
[33]S. R. Mishra, T. R. Cummins, G. D. Waddill, W. J. Gammon, G. van der Laan, K.W. Goodman, and J. G. Tobin, Phys. Rev. Lett. **81**, 1306 (1998).
[34]Emiliana Damian, Undergraduate Research Project, Uppsala University, Uppsala, Sweden (unpublished) (2001).
[35]L. Duda [http://homepage.mac.com/lcduda/RIPES1.html].
[36]P. A. Dowben, Surf. Sci. Rep. **40**, 151 (2000).